New Journal of Physics
The open access journal at the forefront of physics

Deutsche Physikalische Gesellschaft DPG IOP Institute of Physics

PAPER • OPEN ACCESS

Mott polaritons in cavity-coupled quantum materials

To cite this article: Martin Kiffner *et al* 2019 *New J. Phys.* **21** 073066

New Journal of Physics
The open access journal at the forefront of physics

Deutsche Physikalische Gesellschaft DPG
IOP Institute of Physics

Published in partnership with: Deutsche Physikalische Gesellschaft and the Institute of Physics

OPEN ACCESS

RECEIVED
3 May 2019

REVISED
25 June 2019

ACCEPTED FOR PUBLICATION
12 July 2019

PUBLISHED
31 July 2019

PAPER

Mott polaritons in cavity-coupled quantum materials

Martin Kiffner[1,2], **Jonathan Coulthard**[2], **Frank Schlawin**[2], **Arzhang Ardavan**[2] **and Dieter Jaksch**[1,2]

[1] Centre for Quantum Technologies, National University of Singapore, 3 Science Drive 2, 117543, Singapore
[2] Clarendon Laboratory, University of Oxford, Parks Road, Oxford OX1 3PU, United Kingdom

Keywords: quantum materials, Mott insulators, Hubbard model, cavity methods, optical conductivity, polaritons, collective and cooperative effects

Abstract

We show that strong electron–electron interactions in quantum materials can give rise to electronic transitions that couple strongly to cavity fields, and collective enhancement of these interactions can result in ultrastrong effective coupling strengths. As a paradigmatic example we consider a Fermi–Hubbard model coupled to a single-mode cavity and find that resonant electron-cavity interactions result in the formation of a quasi-continuum of polariton branches. The vacuum Rabi splitting of the two outermost branches is collectively enhanced and scales with $g_{\rm eff} \propto \sqrt{2L}$, where L is the number of electronic sites, and the maximal achievable value for $g_{\rm eff}$ is determined by the volume of the unit cell of the crystal. We find that $g_{\rm eff}$ for existing quantum materials can by far exceed the width of the first excited Hubbard band. This effect can be experimentally observed via measurements of the optical conductivity and does not require ultrastrong coupling on the single-electron level. Quantum correlations in the electronic ground state as well as the microscopic nature of the light–matter interaction enhance the collective light–matter interaction compared to an ensemble of independent two-level atoms interacting with a cavity mode.

1. Introduction

Collective phenomena in light–matter interactions are of tremendous interest in quantum physics. The characteristic feature of these phenomena is that observable quantities increase with the number of emitters, and thus intrinsically small quantum effects can be elevated to a macroscopic level. One of the first studied examples is superradiance within the Dicke model [1, 2], which comprises an ensemble of independent two-level atoms interacting with a single mode of the radiation field.

Collective light–matter interactions are conveniently described within the framework of polaritons, which are combined excitations of light and matter. A prominent example is given by dark-state polaritons in laser-driven atomic gases [3] and more recently, polaritons have been investigated in various solid state systems coupled to cavities [4–20]. For example, Bose–Einstein condensation of exciton polaritons in semiconductor materials attracted considerable attention [4, 5], and molecular systems [6–8] coupled to cavities can exhibit giant Rabi splittings between polariton branches. The strong coupling of magnetic excitations to microwave cavities was investigated in [9–14], and two-dimensional electron gases coupled to THz cavities were studied in [15–20]. In all these systems [4–20], Coulomb interactions between electrons play a minor role and are not directly involved in the formation of polaritons.

A particularly intriguing yet challenging platform for investigating light–matter interactions are quantum materials [21–24]. In these systems strong electron–electron interactions give rise a plethora of physical effects that are difficult to describe due to their intrinsically quantum many-body nature. An example is given by the Mott metal–insulator transition [25, 26] which can be modelled within the Fermi–Hubbard model [27].

First steps investigating how quantum materials couple to classical and quantum light have been undertaken recently. The interaction of quantum materials with strong, classical light fields was investigated in [28–31], and superradiance of quantum materials coupled to a cavity field was predicted in [32]. The possibility of inducing superconductivity by coupling electron systems to terahertz and microwave cavities was explored in [33–36].

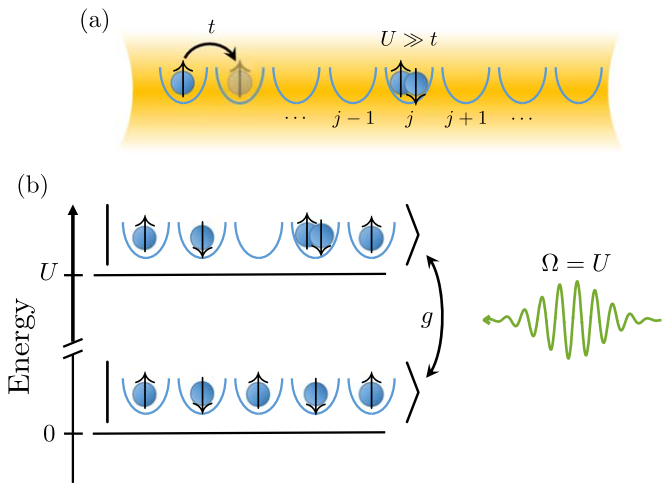

Figure 1. (a) The system of interest comprises an electronic system that is weakly coupled to a single-mode cavity with resonance frequency ω_c and photon energy $\Omega = \hbar\omega_c$. We consider a one-dimensional Fermi–Hubbard model with on-site interaction U and hopping amplitude t for the electronic system. (b) Schematic illustration of the resonant electron–photon coupling with coupling strength g between the electronic ground state and a doublon-holon pair state with energy U.

Furthermore, it was shown in [37, 38] that second-order electron-cavity interactions reduce the magnetic exchange energy in cavity-coupled quantum materials and lead to a collectively enhanced momentum-space pairing effect for electrons.

Here we show that strong electron–electron interactions in quantum materials can give rise to electronic transitions that couple strongly to cavity fields. Collective enhancement of these interactions results in ultrastrong effective coupling strengths that can change the macroscopic properties of the quantum material. As a canonical example we consider a one-dimensional Hubbard model coupled to a single-mode cavity as shown in figure 1(a). We find that the optical conductivity of this system features two peaks that are separated in energy by the collectively enhanced vacuum Rabi frequency $g_{\rm eff} \propto \sqrt{2L}$, where L is the number of electronic sites. Macroscopically large energy splittings are thus even possible for weakly coupled electron–photon systems. The largest possible value of $g_{\rm eff}$ is attained if the material fills the entire cavity. In this case, the effective coupling constant becomes independent of L and $g_{\rm eff} \propto 1/\sqrt{v_{\rm uc}}$, where $v_{\rm uc}$ is the volume of the unit cell of the crystal. As an example, for the quantum material ET-F_2TCNQ, which is well described by a one-dimensional Hubbard model, $g_{\rm eff}$ can exceed 250 meV. This is several orders of magnitude larger than collective energy shifts in atomic systems [39–41] and comparable to the extremely large energy splittings achieved in cavity-coupled molecular materials [6–8].

The resonant light–matter interactions considered here are schematically shown in figure 1(b). An electronic state at half filling and with no electronic excitation is resonantly coupled via a cavity photon to an electronic state with one doubly occupied state (doublon) and an empty site (holon) next to it. These states differ in energy by the on-site Coulomb interaction U, which corresponds to the Mott gap of the quantum material. The transition dipole moment between these two states is of the order of $d\,e$ (d: lattice spacing, e: elementary charge), which is comparable to strong transitions in alkali metal atoms [42]. We find that the resonant coupling of this transition with a single-mode cavity gives rise to polariton states.

Note that the underlying principle of this effect is that strong electron–electron interactions split the electronic energy levels into different bands. Transitions between these bands can exhibit large dipole moments and couple strongly to cavity fields. In this sense our results are quite generic and do not only apply to the system shown in figure 1(a), but to quantum materials with strong on-site electron–electron interactions in general. In the special case studied here, the resonant electron–photon interactions lead to a quasi-continuum of polariton states, and the two branches with the largest energy splitting $g_{\rm eff}$ can be constructed from the electronic ground state. The collective energy splitting $g_{\rm eff} \propto \sqrt{2L}$ of these branches gives rise to the two peaks in the optical conductivity.

Our scheme is qualitatively different to conventional quantum optics systems like the Dicke model [1, 2, 43, 44] where dipole transitions of non-interacting atoms couple collectively to the cavity field. Comparing our system with the Dicke model reveals two important features of our scheme. First, the quantum correlations in the ground state of the electronic system lead to an enhancement of $g_{\rm eff}$ by $\approx$18%. Second, $g_{\rm eff}$ for the electronic system is larger by a factor of $\sqrt{2}$ than in the Dicke model. We show that this difference is caused by the different microscopic nature of the light–matter coupling in these systems.

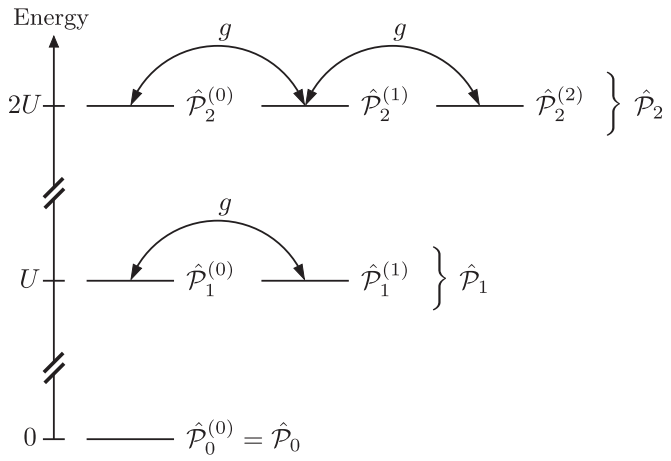

Figure 2. Schematic drawing of the spectrum of $\hat{H}_0 = \hat{D} + \hat{P}$ for $U = \Omega$. $\hat{\mathcal{P}}_n^{(j)}$ projects onto a sub-manifold with j photons and $n - j$ doublons, and $\hat{\mathcal{P}}_n$ is the projector onto the manifold with n excitations. Only manifolds with $n \leqslant 2$ excitations are shown. The resonant cavity coupling g between sub-manifolds is indicated by arrows. Higher-order couplings induced by $\hat{V}$ are not shown.

This paper is organised as follows. The theoretical model describing the system shown in figure 1(a) is introduced in section 2. Our results are presented in section 3, and the derivation of the Mott polaritons in the manifold with one excitation is outlined in section 3.1. We then show in section 3.2 that a direct signature of the light–matter hybridisation appears in the optical conductivity. The discussion in section 4 gives an intuitive explanation for the collective enhancement of the polariton splitting and illustrates similarities and differences of our system with the Dicke model. The experimental observation of the predicted effects is discussed in section 5, and a summary of our results is provided in section 6.

2. Model

In this section we present the theoretical model established in [37, 38] for the quantum hybrid system shown in figure 1(a). The electronic system is described by the one-dimensional Fermi–Hubbard model [27] with on-site energy U and hopping amplitude t. The electrons are weakly coupled to a single-mode cavity with resonance frequency ω_c, and $\Omega = \hbar\omega_c$ is the photon energy.

The gross energy structure of our system in the parameter regime of interest ($U, \Omega \gg t$) is determined by the Hamiltonian

$$\hat{H}_0 = \hat{P} + \hat{D}, \tag{1}$$

where

$$\hat{P} = \Omega \hat{a}^\dagger \hat{a} \tag{2}$$

describes the cavity photons and $\hat{a}^\dagger$ ($\hat{a}$) is the bosonic photon creation (annihilation) operator. The operator $\hat{D}$ in equation (1) accounts for the on-site Coulomb repulsion between electrons

$$\hat{D} = U \sum_{k=0}^{L} k\, \hat{\mathcal{P}}_k^D, \tag{3}$$

where U is the interaction energy and $\hat{\mathcal{P}}_k^D$ is the projector onto the manifold with k doubly-occupied sites [37]. In the following we refer to these excitations as doublons. The eigenstates of $\hat{H}_0$ are tensor products of photon number states $|j_P\rangle$ with j photons and Wannier states [27] with k doublons. The associated eigenvalues $j\Omega + kU$ are generally highly degenerate and form manifolds as shown in figure 2. We denote the projector onto a manifold with j photons and $k = n - j$ doublons by

$$\hat{\mathcal{P}}_n^{(j)} = \hat{\mathcal{P}}_{n-j}^D \otimes \hat{\mathcal{P}}_j^P, \tag{4}$$

where n is the total number of excitations, $\hat{\mathcal{P}}_j^P = |j_P\rangle\langle j_P|$ projects onto the subspace with j photons and

$$\hat{\mathcal{P}}_n = \sum_{j=0}^{n} \hat{\mathcal{P}}_n^{(j)} \tag{5}$$

projects onto all sub-manifolds with n excitations.

Modifications to the simple energy structure shown in figure 1 arise from the electron hopping and the electron–photon interaction. The hopping operator is

$$\hat{T} = -t \sum_{\langle jk \rangle \sigma} (\hat{c}^{\dagger}_{j,\sigma} \hat{c}_{k,\sigma} + \text{h.c.}), \tag{6}$$

where $\langle jk \rangle$ denotes neighbouring sites with $j < k$ and $\hat{c}^{\dagger}_{j,\sigma}$ ($\hat{c}_{j,\sigma}$) creates (annihilates) an electron at site j in spin state $\sigma \in \{\uparrow,\downarrow\}$.

The electron–photon interaction was derived in [37, 38] via the Peierls substitution [27] and by expanding the resulting interaction Hamiltonian up to second order in the electron-cavity coupling

$$\hat{V} = g(\hat{a} + \hat{a}^{\dagger})\hat{\mathcal{J}} - \frac{1}{2}\frac{g^2}{t^2}(\hat{a} + \hat{a}^{\dagger})^2 \hat{T}, \tag{7}$$

where

$$\hat{\mathcal{J}} = -\mathrm{i} \sum_{\langle jk \rangle \sigma} (\hat{c}^{\dagger}_{j,\sigma} \hat{c}_{k,\sigma} - \hat{c}^{\dagger}_{k,\sigma} \hat{c}_{j,\sigma}) \tag{8}$$

is the dimensionless current operator. The parameter $g = t\eta$ in $\hat{V}$ determines the coupling strength between the electrons and photons, and

$$\eta = \frac{de}{\sqrt{2\hbar\varepsilon_0 \omega_c \nu}} \tag{9}$$

is a dimensionless parameter that depends on the lattice constant d and the cavity mode volume ν (e: elementary charge, ε_0: vacuum permittivity, $\hbar$: reduced Planck's constant). The derivation of $\hat{V}$ assumes $\eta \ll 1$, and this condition is also required to grant the validity of the single-mode cavity approximation [45].

With the preceding definitions we arrive at the total Hamiltonian for the quantum hybrid system in figure 1

$$\hat{H} = \hat{H}_0 + \hat{H}_1, \tag{10}$$

where

$$\hat{H}_1 = \hat{T} + \hat{V}, \tag{11a}$$

$$= \left[1 - \frac{1}{2}\frac{g^2}{t^2}(\hat{a} + \hat{a}^{\dagger})^2\right]\hat{T} + g(\hat{a} + \hat{a}^{\dagger})\hat{\mathcal{J}}. \tag{11b}$$

For the parameters of interest (U, $\Omega \gg t \gg g$), H_1 can be treated as a perturbation to the gross energy structure dictated by H_0. The general effective Hamiltonian $\hat{H}_{\text{eff}}$ corresponding to $\hat{H}$ can be written as

$$\hat{H}_{\text{eff}} = \sum_{n=0} \hat{H}^{(n)}_{\text{eff}} \hat{\mathcal{P}}_n, \tag{12}$$

where $\hat{H}^{(n)}_{\text{eff}}$ is the effective Hamiltonian in subspace $\hat{\mathcal{P}}_n$ [46].

In the following section 3 we investigate the formation of Mott polaritons through resonant electron–photon interactions in $\hat{\mathcal{P}}_1$. To set the stage for this we recall how the cavity modifies the physics in $\hat{\mathcal{P}}_0$, which was investigated in [37, 38] using second-order perturbation theory. For the special case of $\Omega = U$ and an electronic system at half filling, the effective Hamiltonian in $\hat{\mathcal{P}}_0$ is given by [37, 38]

$$\hat{H}^{(0)}_{\text{eff}} = \hat{H}_{\text{S}} \otimes \hat{\mathcal{P}}^{P}_0, \tag{13}$$

where

$$\hat{H}_{\text{S}} = -J_c \hat{\mathcal{P}}^{D}_0 \left(\sum_{\langle kl \rangle} \hat{b}^{\dagger}_{kl} \hat{b}_{kl} \right) \hat{\mathcal{P}}^{D}_0 \tag{14}$$

and

$$\hat{b}^{\dagger}_{kl} = (\hat{c}^{\dagger}_{k,\uparrow} \hat{c}^{\dagger}_{l,\downarrow} - \hat{c}^{\dagger}_{k,\downarrow} \hat{c}^{\dagger}_{l,\uparrow})/\sqrt{2} \tag{15}$$

creates a singlet pair at sites k and l. $\hat{H}_{\text{S}}$ acts only on the electronic system and is an isotropic Heisenberg model (see appendix A) with coupling

$$J_c = \mathcal{R}_c \frac{4t^2}{U}, \tag{16}$$

where

$$\mathcal{R}_c = 1 - \frac{1}{2}\frac{g^2}{t^2} \tag{17}$$

is a dimensionless scaling factor. Note that R_c is equal to unity for $g = 0$ and $R_c < 1$ for $g > 0$, and thus the cavity reduces the magnetic exchange interaction. In addition, we have $J_c > 0$ for all permitted values of $g \ll t$ and thus the ground state $|G\rangle$ of $\hat{H}_S$ is an antiferromagnetic state [27].

3. Results

Throughout this section we consider an electronic system at half filling and $\Omega = U$. In section 3.1 we show that resonant electron–photon interactions result in the formation of polaritons, and the energy splitting of the two outermost polariton branches is collectively enhanced. Evidence for this light–matter hybridisation can be found in the optical conductivity as shown in section 3.2.

3.1. Mott polaritons

The first excited manifold $\hat{\mathcal{P}}_1$ contains all states with either one doublon or one photon. The effective Hamiltonian in $\hat{\mathcal{P}}_1$ and in first order in H_1 is (see appendix B)

$$\hat{H}_{\rm eff}^{(1)} = U\hat{\mathcal{P}}_1 + \mathcal{R}_c\hat{\mathcal{P}}_1^{(0)}\hat{T}\hat{\mathcal{P}}_1^{(0)} + \hat{H}_{D-P}. \tag{18}$$

Higher-order terms in H_1 are neglected in equation (18) and become negligible in the limit $U \gg t, g$. The first term in equation (18) is a constant energy offset of the states in $\hat{\mathcal{P}}_1$. The second term describes the dynamics of the doublon and holon in $\hat{\mathcal{P}}_1$ and gives rise to the first excited Hubbard band. At $g = 0$, the width of this band is $8t$ [47, 48], and the scaling factor $\mathcal{R}_c$ reduces this width slightly for $g > 0$. The last term in equation (18) accounts for the resonant doublon-photon interaction and is given by (see appendix C)

$$\hat{H}_{D-P} = g(\hat{\mathcal{D}}^\dagger \otimes \hat{\mathcal{A}} + \hat{\mathcal{D}} \otimes \hat{\mathcal{A}}^\dagger), \tag{19}$$

where

$$\hat{\mathcal{A}} = |0_P\rangle\langle 1_P| \tag{20}$$

is a transition operator between the vacuum and the one-photon state and

$$\hat{\mathcal{D}} = \hat{\mathcal{P}}_0^D\hat{\mathcal{J}}\hat{\mathcal{P}}_1^D \tag{21}$$

mediates a transition between one and zero doublon states. We note that the definition of $\hat{\mathcal{J}}$ allows us to write $\hat{\mathcal{D}}$ as

$$\hat{\mathcal{D}} = -\mathrm{i}(\hat{\mathcal{D}}_R - \hat{\mathcal{D}}_L), \tag{22}$$

where

$$\hat{\mathcal{D}}_R = \hat{\mathcal{P}}_0^D\left(\sum_{\langle jk\rangle\sigma}\hat{c}_{j,\sigma}^\dagger\hat{c}_{k,\sigma}\right)\hat{\mathcal{P}}_1^D \tag{23a}$$

$$\hat{\mathcal{D}}_L = \hat{\mathcal{P}}_0^D\left(\sum_{\langle jk\rangle\sigma}\hat{c}_{k,\sigma}^\dagger\hat{c}_{j,\sigma}\right)\hat{\mathcal{P}}_1^D. \tag{23b}$$

Since $j < k$ in $\langle jk\rangle$, this means that $\hat{\mathcal{D}}_R$ ($\hat{\mathcal{D}}_R^\dagger$) annihilates (creates) a doublon-holon pair where the doublon is to the right of the holon. Similarly, $\hat{\mathcal{D}}_L$ ($\hat{\mathcal{D}}_L^\dagger$) annihilates (creates) a doublon-holon pair where the doublon is to the left of the holon.

We emphasise that $\hat{H}_{D-P}$ is of first order in the electron–photon coupling since it is proportional to the coupling strength g. This is in contrast to the ground-state manifold where the leading term is of second order in the electron–photon coupling [37, 38]. We thus expect that the electron-cavity coupling has a much stronger effect in $\hat{\mathcal{P}}_1$ than in $\hat{\mathcal{P}}_0$ for a fixed value of g.

The resonant electron–photon coupling described by $\hat{H}_{D-P}$ in equation (19) results in the formation of doublon-photon polaritons. All eigenstates of $\hat{H}_{D-P}$ with non-zero eigenvalues can be constructed from the eigenstates of $\hat{H}_S$ with non-zero eigenvalues (see appendix C). For each eigenstate $|g_j\rangle$ with

$$\hat{H}_S|g_j\rangle = \mathcal{E}_j|g_j\rangle \tag{24}$$

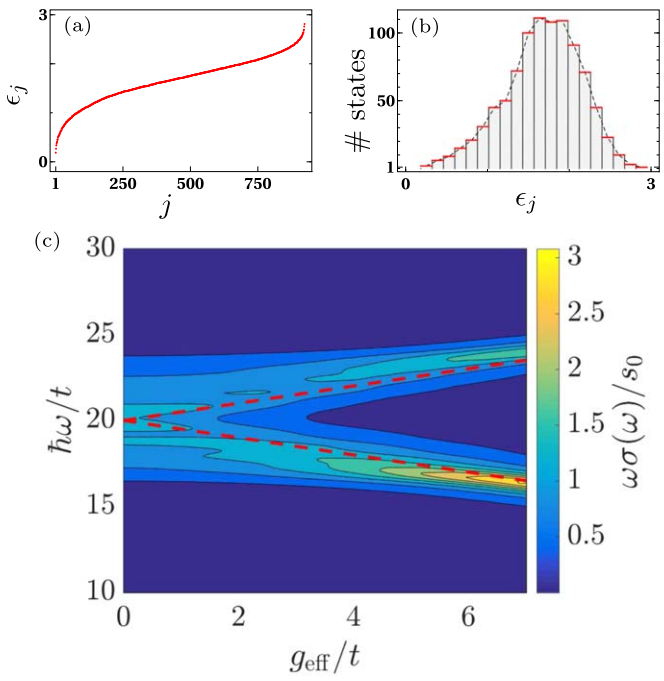

Figure 3. (a) All values of ϵ_j for a system with $L = 12$ sites at half filling and total spin $S = 0$. (b) Density of states of the ϵ_j values shown in (a). (c) Density plot of $\omega\sigma(\omega)$ for $L = 12$ sites at half filling, zero temperature and $U = \Omega = 20t$, where $\sigma(\omega)$ is the optical conductivity and $s_0 = te^2/(\hbar^2 d)$. $g_{\rm eff} = 3.33g\sqrt{L}$ is the collective coupling strength, and the red dashed lines indicate the energies $\pm 0.5 g_{\rm eff}$ of $|\psi^{\rm max}_{D-P}\rangle_\pm$. Each term of the sum in equation (30) was artificially broadened with a Lorentzian of width $0.5t$.

and $\mathcal{E}_j < 0$ the corresponding pair of polariton states is

$$|\psi^j_{D-P}\rangle_\pm = \frac{1}{\sqrt{2}}\left[|g_j\rangle \otimes |1_P\rangle \pm \frac{1}{2\epsilon_j}(\hat{\mathcal{D}}^\dagger|g_j\rangle) \otimes |0_P\rangle\right], \tag{25}$$

where

$$\epsilon_j = \sqrt{-\mathcal{E}_j/J_c} \tag{26}$$

is a rescaled eigenvalue of $\hat{H}_{\rm S}$ with $\epsilon_j > 0$ and

$$\hat{H}_{D-P}\,|\psi^{(j)}_{D-P}\rangle_\pm = \pm 2g\epsilon_j\,|\psi^{(j)}_{D-P}\rangle_\pm. \tag{27}$$

Each polariton state in equation (25) is a maximally entangled superposition of a state with one doublon and no photon, and a state with no doublon and one photon. The largest value $\epsilon_{\rm max}$ corresponds to the ground state $|G\rangle$ of $\hat{H}_{\rm S}$ in equation (13) with energy $\mathcal{E}_G$, and thus

$$\epsilon_{\rm max} = \sqrt{-\mathcal{E}_G/J_c} \approx \sqrt{L\log 2} \tag{28}$$

for $L \gg 1$, see appendix A. The energy difference between the corresponding polariton states $|\psi^{\rm max}_{D-P}\rangle_\pm$ is

$$g_{\rm eff} = 4g\sqrt{L\log 2} \approx 3.33g\sqrt{L}, \tag{29}$$

and carries a direct signature of the collective doublon-photon coupling. Note that we also provide an approximate but intuitive derivation for the value of $g_{\rm eff}$ in section 4.

An upper bound for $g_{\rm eff}$ can be obtained by assuming that the material fills the mode volume v of the cavity such that $v = Lv_{\rm uc}$, where $v_{\rm uc}$ is the volume per lattice site. Furthermore, we assume $v \lesssim \lambda_c^3$ (λ_c: cavity wavelength) such that the spatial dependence of the cavity mode function is small and $g = \eta t \propto 1/\sqrt{v}$. It follows that the value of $g_{\rm eff}$ is independent of L and just depends on $v_{\rm uc}$.

The values of ϵ_j for a system with $L = 12$ sites are shown in figure 3(a), and the corresponding density of states is shown in figure 3(b). Even a relatively small system with $L = 12$ sites exhibits a quasi-continuum of polariton states, with the largest density of states for intermediate values of ϵ_j.

Note that the states $|\psi^j_{D-P}\rangle_\pm$ in equation (25) are not eigenstates of the full effective Hamiltonian in equation (18) due to the kinetic energy term $\hat{\mathcal{P}}^{(0)}_1\hat{T}\hat{\mathcal{P}}^{(0)}_1$. However, we show in appendix C that the states $|\psi^j_{D-P}\rangle_\pm$ are approximate eigenstates of $\hat{H}^{(1)}_{\rm eff}$ if their energy splitting is much larger than t. In this case, $\hat{\mathcal{P}}^{(0)}_1\hat{T}\hat{\mathcal{P}}^{(0)}_1$ only leads to a broadening of the polariton states by coupling them off-resonantly to the quasi-continuum of the first Hubbard band.

3.2. Optical conductivity

A direct signature of the collective doublon-photon coupling in the first excited manifold can be found in the optical conductivity [27]

$$\sigma(\omega) = \frac{\pi e^2 t^2}{d\hbar^3} \sum_{m>0} \frac{|\langle\psi_m|\hat{\mathcal{J}}|\psi_0\rangle|^2}{\omega_m - \omega_0} \delta[\omega - (\omega_m - \omega_0)], \tag{30}$$

where $|\psi_m\rangle$ are the eigenstates of the full Hamiltonian $\hat{H}$ with energies $E_m = \hbar\omega_m$ and $E_0 = \hbar\omega_0$ is the energy of the ground state $|\psi_0\rangle$. We calculate the optical conductivity with the full system Hamiltonian using Krylov subspace methods [49] for a half-filled electronic system with $L = 12$ sites. Figure 3(c) shows a density plot of the optical conductivity spectrum as a function of $g_{\rm eff}$ and ω. At $g_{\rm eff} = 0$ the optical conductivity maps out the first excited Hubbard band of width $8t$ that describes the kinematic excitations of a single doublon. At $g_{\rm eff}/t \approx 3$ the optical conductivity splits into two branches that become narrower with increasing $g_{\rm eff}$. The peaks of the optical conductivity signal approximately follow the energies of the polariton branches $|\psi^{\rm max}_{D-P}\rangle_\pm$.

These results suggest that the optical conductivity signal is mostly dominated by the two outermost polariton branches $|\psi^{\rm max}_{D-P}\rangle_\pm$ for $g_{\rm eff}/t \geqslant 3$ which can be understood as follows. States which are split strongly by the cavity's light field are also expected to couple strongly to an externally applied light field, and thus they show a strong signal in the optical conductivity. This can also be confirmed by noting that $|\psi_m\rangle = |\psi^{\rm max}_{D-P}\rangle_\pm$ are the only polariton states contributing to the sum in equation (30) if we approximate the ground state by $|\psi_0\rangle \approx |G\rangle \otimes |0_P\rangle$. The finite width of the optical conductivity signal is caused by the coupling of polariton states to the first Hubbard band via $\hat{\mathcal{P}}_1^{(0)}\hat{T}\hat{\mathcal{P}}_1^{(0)}$, and this coupling becomes less effective with increasing energy splitting $\propto g_{\rm eff}$ (see appendix C). The slight asymmetry in the intensity and position of the two conductivity branches as well as the slight increase of the energy splitting compared with the analytical result is a consequence of the higher order terms that are neglected in equation (18) but taken into account in the numerical evaluation of $\sigma(\omega)$.

4. Discussion

In section 3 we have shown that there is a one-to-one correspondence between the polariton branches in the manifold $\hat{\mathcal{P}}_1$ and the eigenstates of $\hat{H}_{\rm S}$ in equation (14) with zero excitations. The two branches with the largest splitting $g_{\rm eff}$ contribute significantly to the optical conductivity signal and correspond to the electronic ground state $|G\rangle$ of $\hat{H}_{\rm S}$. A rigorous derivation of the results presented in section 3 is provided in appendix C. Here we give an alternative and approximate derivation of the two polariton branches with the largest energy splitting $g_{\rm eff}$. This more intuitive picture allows us to gain further insights into our system and highlights similarities and differences with other polariton systems.

Our elementary derivation of $g_{\rm eff}$ starts by approximating the electronic ground state $|G\rangle$ of $\hat{H}_{\rm S}$ by $|G\rangle \approx |G_{\rm Néel}\rangle$, where

$$|G_{\rm Néel}\rangle = |\uparrow_1, \downarrow_2, \uparrow_3, \ldots\rangle \tag{31}$$

is the antiferromagnetic Néel state. Note that we also employed this state for $L = 5$ to illustrate the electronic ground state in figure 1(b). Applying the doublon-holon creation operator $\hat{\mathcal{D}}^\dagger$ (see equation (21)) to this state results in a state with one doublon excitation,

$$|E_{\rm Néel}\rangle = {\rm i}\mathcal{C}(\hat{\mathcal{D}}_R^\dagger - \hat{\mathcal{D}}_L^\dagger)|G_{\rm Néel}\rangle, \tag{32}$$

where $\mathcal{C}$ is a normalisation constant. Assuming open boundary conditions, the operators $\hat{\mathcal{D}}_L^\dagger$ and $\hat{\mathcal{D}}_R^\dagger$ each create $L-1$ states with a holon-doublon pair. Since all these states are orthonormal, we have $\mathcal{C} = 1/\sqrt{2(L-1)} \approx 1/\sqrt{2L}$ for $L \gg 1$. Ignoring boundary effects the matrix element of $\hat{H}_{D-P}$ between the states $|G_{\rm Néel}\rangle \otimes |1_P\rangle$ and $|E_{\rm Néel}\rangle \otimes |0_P\rangle$ is thus

$$[\langle E_{\rm Néel}| \otimes \langle 0_P|]\hat{H}_{D-P}[|G_{\rm Néel}\rangle \otimes |1_P\rangle] \approx g\sqrt{2L}. \tag{33}$$

Diagonalisation of $\hat{H}_{D-P}$ in the two-dimensional subspace spanned by $|G_{\rm Néel}\rangle \otimes |1_P\rangle$ and $|E_{\rm Néel}\rangle \otimes |0_P\rangle$ results in two polariton states with energy splitting

$$g_{\rm eff}[\text{Néel}] = 2g\sqrt{2L}. \tag{34}$$

This value needs to be compared to $g_{\rm eff}$ in equation (29). We find that $g_{\rm eff}$ is larger than $g_{\rm eff}[\text{Néel}]$ by a factor of $\sqrt{2\log 2} \approx 1.18$, i.e. $g_{\rm eff}/g_{\rm Néel}[\text{Néel}] = \sqrt{2\log 2}$. The reason for this is that $|G_{\rm Néel}\rangle$ is not the true ground state of the electronic system, which is an entangled superposition of Wannier states. It follows that the correlations in the true ground state of the electronic system enhance the polariton splitting by about 18%.

Next we compare our results to those obtained for L independent two-level atoms with transition energy U that interact resonantly with a single cavity mode. This model is a special case of the so-called Tavis–Cummings

[43, 44] or Dicke [1] model, and in the following we refer to it as the Dicke model. A brief description of the Dicke Hamiltonian is given in appendix D. The manifold with zero excitations has only one non-degenerate ground state where the cavity is in the vacuum state and all atoms are in the ground state. The manifold with one excitation contains two states that are split by (see appendix D)

$$g_{\rm eff}\,[\text{Dicke}] = 2g\sqrt{L}\,, \tag{35}$$

which is smaller than $g_{\rm eff}$ [Néel] in equation (34) by a factor of $\sqrt{2}$. This difference can be attributed to the different nature of the light–matter interaction for atoms and electrons: The cavity field couples to the atomic density in the Dicke model, whereas the light–matter coupling in the electronic system is proportional to the current operator. Starting from $|G_{\rm Néel}\rangle$ the operator $\hat{H}_{D-P}$ can create a doublon with the holon either to the left or two the right, giving rise to $2L$ possible states as discussed above. On the contrary, the corresponding Hamiltonian for the atoms can only locally excite one atom at site k, and there are only L different states. Taking into account the normalisation of the corresponding states gives rise to collective coupling strengths proportional to $\sqrt{2L}$ in the case of electrons and $\sqrt{L}$ in the case of atoms.

5. Experimental realisation

To discuss the experimental observation of the collectively enhanced light–matter coupling in our system we consider ET-F_2TCNQ [50–53], which is a generic example of a one-dimensional Mott insulator where $U \gg t$. The optical conductivity σ is the central materials quantity of interest since it determines the dielectric function of the material and thus its reflectivity and transmittance, for example. Typical experiments measure the optical conductivity indirectly, e.g. via reflectivity measurements and self-consistent calculations utilising Kramers–Kronig relations [53]. Optimal strategies for measuring σ depend on the specifics of the experimental setup and are beyond the scope of this work.

In order to observe the splitting of the optical conductivity spectrum shown in figure 3 we require $g_{\rm eff}/t \gtrsim 3$. In addition, the photon-doublon coupling must be much faster than the cavity decay rate κ, i.e. $g_{\rm eff} \gg \hbar\kappa$. In the case of ET-$F_2$TCNQ [50] we find $g_{\rm eff}/t \approx 6.4$. It follows that the two branches in the optical conductivity should be clearly visible, and their energy splitting can be as large as $g_{\rm eff} \approx 250$ meV. Even larger values of $g_{\rm eff}/t$ are possible in materials with a smaller Mott gap or smaller unit cells. The condition $g_{\rm eff} \gg \hbar\kappa$ is also fulfilled in ET-F_2TCNQ where $t/\hbar \approx 2\pi \times 10$ THz [50, 51], which is at least two orders of magnitude larger than cavity decay rates of lossy microcavities with frequencies in the low THz regime [54].

Finally we address the finite lifetime τ_D of doublon excitations which increases exponentially with U/t [55]. The experimentally measured value for ET-F_2TCNQ at ambient pressure is $\tau_D \approx 0.5$ ps [53], which corresponds to a decay rate of $\kappa_D \approx 0.2t/\hbar$. This decay rate is smaller than the artificial broadening introduced in the numerical evaluation of equation (30), where each term of the sum was broadened with a Lorentzian of width $0.5t/\hbar$. We thus conclude that the finite lifetime of doublons does not hinder the observation of the two peaks in the optical conductivity.

6. Summary

We have shown that the resonant coupling between strongly correlated electrons and a single-mode cavity results in the formation of Mott polaritons. The manifold with one excitation exhibits a dense spectrum of polariton branches which can be derived from the eigenstates in the zero excitation manifold. At half filling the effective Hamiltonian in the manifold with zero excitations is an isotropic Heisenberg chain. Each eigenstate with non-zero eigenvalue $\mathcal{E}_j < 0$ gives rise to two polariton branches, and the magnitude of their energy splitting is proportional to $\sqrt{-\mathcal{E}_j}$. The two branches with the largest energy splitting are thus associated with the ground state of the isotropic Heisenberg chain, and their energy splitting $g_{\rm eff}$ is proportional to $\sqrt{2L}$, where L is the number of electronic sites.

An approximate derivation for $g_{\rm eff}$ in section 4 illustrates that quantum correlations in the ground state result in an enhancement of the polariton splitting by 18%. Furthermore, $g_{\rm eff} \propto \sqrt{2L}$ is a direct consequence of the fact that the electron–photon interaction is mediated by the current operator. The absorption of a photon is associated with an electronic hopping process creating a holon-doublon pair where the doublon is either to the right or the left of the holon. This two-fold excitation pathway is in contrast to atomic systems where the atomic density couples to the cavity field, allowing only for one local excitation when absorbing a photon. The collective polariton splitting for L independent two-level atoms and in the manifold with one excitation is consequently smaller by a factor of $\sqrt{2}$ compared to our electronic system.

We find that the collectively enhanced polariton splitting is directly observable in the optical conductivity, which features two peaks separated by $g_{\rm eff} \propto \sqrt{2L}$. If the material fills the whole mode volume of the cavity, the

magnitude of the splitting is independent of the mode volume and just depends on $1/\sqrt{v_{\rm uc}}$, where $v_{\rm uc}$ is the volume of the unit cell of the crystal. As a generic example of a one-dimensional Mott insulator we consider ET-F_2TCNQ, and find that its unit cell is small enough such that the splitting of the optical conductivity signal exceeds the width of the first Hubbard band. The optical conductivity thus carries a clear signature of the collective electron–photon coupling.

We emphasise that $g_{\rm eff} \propto 1/\sqrt{v_{\rm uc}}$ together with the small unit cells in solid state materials can result in macroscopically large polariton splittings $g_{\rm eff}$. In the case of ET-F_2TCNQ, we find $g_{\rm eff} \approx 250$ meV, which is several orders of magnitude larger than what has been achieved in atomic systems [39–41]. In addition, we note that the near-resonant electron–photon coupling described in this work is much larger than the effects described in [37, 38], which are mediated by virtual, second-order electron–photon interactions.

In this paper we focused on the resonant electron–photon coupling in the manifold with one excitation. In conventional quantum optics systems like the Dicke model one can approximately diagonalize the Hamiltonian in several excitation subspaces simultaneously via bosonization techniques. Since this approach is in general not applicable to our fermionic system [27], it is an intriguing yet challenging prospect for future studies to investigate near-resonant electron–photon interactions in higher-excited manifolds, see figure 2. Since the electron–photon interaction increases with the number of photons j as $\sqrt{j}$, the energy spectrum is anharmonic. Like in atomic systems [56] this feature results in giant photon nonlinearities and further amplifies the intrinsically large optical nonlinearity of Mott insulators [57]. Furthermore, the physics in manifolds with a large number of excitations will be fundamentally different from the Dicke model. The reason is that the maximal number of atomic excitations within the Dicke model is L, but at most $L/2$ doublons can be created in the electronic system.

A further intriguing avenue for future studies is the investigation of higher-dimensional systems. For example, the electron-cavity interaction in higher-dimensional systems can be tuned via the relative orientation between the crystal and the cavity polarisation vector [37, 38]. In k-dimensional systems where the cavity couples to all spatial directions one expects $g_{\rm eff} \propto \sqrt{2k}$ due to the additional excitation pathways to nearest-neighbour sites, and thus a further enhancement of the effective coupling strength.

Acknowledgments

MK and DJ acknowledge financial support from the National Research Foundation, Prime Minister's Office, Singapore, and the Ministry of Education, Singapore, under the Research Centres of Excellence program. DJ, FS and JC acknowledge funding from the European Research Council under the European Union's Seventh Framework Programme (FP7/2007-2013)/ERC Grant Agreement no. 319286, Q-MAC. DJ acknowledges funding from EPSRC grant no. EP/P009565/1. MK, AA and DJ thank Andrea Cavalleri for discussions.

Appendix A. Isotropic Heisenberg model

The effective Hamiltonian $\hat{H}_{\rm S}$ in equation (14) can be cast into the form [27]

$$\hat{H}_{\rm S} = J_c \sum_{\langle jk \rangle} \left(\hat{\boldsymbol{S}}_j \cdot \hat{\boldsymbol{S}}_k - \frac{\hat{n}_j \hat{n}_k}{4} \right) \hat{\mathcal{P}}_0^D, \tag{A1}$$

where $\hat{n}_j = \hat{c}_{j,\uparrow}^\dagger \hat{c}_{j,\uparrow} + \hat{c}_{j,\downarrow}^\dagger \hat{c}_{j,\downarrow}$ is the number operator at site j and the components of the local spin operator $\hat{\boldsymbol{S}}_j = (\hat{S}_x^j, \hat{S}_y^j, \hat{S}_z^j)$ are defined as

$$\hat{S}_x^j = \frac{1}{2}(\hat{c}_{j,\uparrow}^\dagger \hat{c}_{j,\downarrow} + \hat{c}_{j,\downarrow}^\dagger \hat{c}_{j,\uparrow}), \tag{A2a}$$

$$\hat{S}_y^j = \frac{\mathrm{i}}{2}(\hat{c}_{j,\downarrow}^\dagger \hat{c}_{j,\uparrow} - \hat{c}_{j,\uparrow}^\dagger \hat{c}_{j,\downarrow}), \tag{A2b}$$

$$\hat{S}_z^j = \frac{1}{2}(\hat{c}_{j,\uparrow}^\dagger \hat{c}_{j,\uparrow} - \hat{c}_{j,\downarrow}^\dagger \hat{c}_{j,\downarrow}). \tag{A2c}$$

At half filling every site is occupied precisely by one electron, and thus

$$\hat{H}_{\rm S} = J_c \sum_{\langle jk \rangle} \left(\hat{\boldsymbol{S}}_j \cdot \hat{\boldsymbol{S}}_k - \frac{1}{4} \right) \hat{\mathcal{P}}_0^D \tag{A3}$$

is an isotropic spin-1/2 Heisenberg chain with exchange coupling J_c. The ground state energy of $\hat{H}_{\rm S}$ per electron and in the thermodynamic limit ($L \to \infty$) is $\mathcal{E}_G/L = -J_c \log 2$ [58], and thus equation (28) follows.

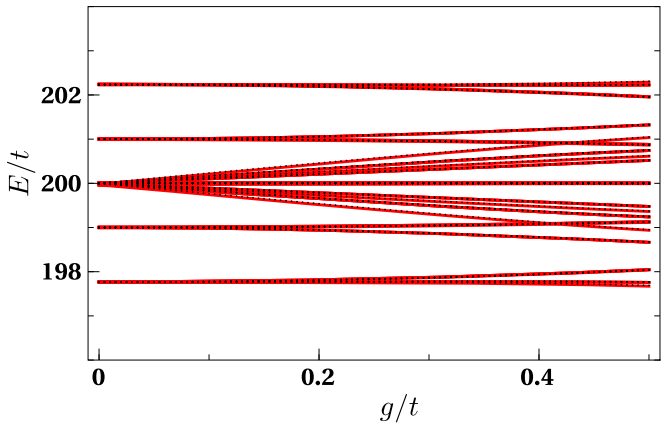

Figure B1. Comparison of the eigenenergies E of the system Hamiltonian $\hat{H}$ in the manifold with one excitation and $\hat{H}_{\rm eff}^{(1)}$ defined in equation (18). We consider a system with $L = 4$ sites at half filling and show E as a function of the cavity coupling g. The eigenvalues corresponding to $\hat{H}$ ($\hat{H}_{\rm eff}^{(1)}$) are shown by red solid (black dotted) lines. The exact diagonalization calculations take into account photon states $|j_p\rangle$ with $j \in \{0,\ 1,\ 2,\ 3,\ 4\}$, and we set $U = \Omega = 200t$.

Appendix B. Effective Hamiltonian in $\hat{\mathcal{P}}_1$

An approximate effective Hamiltonian in the manifold $\hat{\mathcal{P}}_1$ that only takes into account the perturbation $\hat{H}_1$ in first order and for $\Omega = U$ is [46, 27]

$$\hat{H}_{\rm eff}^{(1)} = U\hat{\mathcal{P}}_1 + \hat{\mathcal{P}}_1\hat{H}_1\hat{\mathcal{P}}_1. \tag{B1}$$

The eigenvalues of $\hat{H}_{\rm eff}^{(1)}$ will coincide with the eigenvalues of the full Hamiltonian $\hat{H}$ in $\hat{\mathcal{P}}_1$ in the limit $U \gg g, t$ where higher-order terms in $\hat{H}_1$ are negligible. The first term in equation (B1) represents the unperturbed energy of the manifold with one excitation, which can be either a photon with energy $\Omega = U$ or a doublon. The second term in equation (B1) can be written as

$$\hat{\mathcal{P}}_1\hat{H}_1\hat{\mathcal{P}}_1 = \mathcal{R}_c\hat{\mathcal{P}}_1^{(0)}\hat{T}\hat{\mathcal{P}}_1^{(0)} + g\hat{\mathcal{P}}_1[(\hat{a} + \hat{a}^\dagger)\hat{\mathcal{J}}]\hat{\mathcal{P}}_1, \tag{B2}$$

where we used $\hat{\mathcal{P}}_1^{(1)}\hat{T}\hat{\mathcal{P}}_1^{(1)} = 0$ at half filling. The second term in equation (B2) is

$$g\hat{\mathcal{P}}_1[(\hat{a} + \hat{a}^\dagger)\hat{\mathcal{J}}]\hat{\mathcal{P}}_1 = \hat{H}_{D-P}, \tag{B3}$$

where $\hat{H}_{D-P}$ is defined in equation (19). Combining equations (B1)–(B3) shows that the expression for $\hat{H}_{\rm eff}^{(1)}$ in equation (B1) is the same as equation (18).

A comparison of the eigenvalues of the effective Hamiltonian $\hat{H}_{\rm eff}^{(1)}$ and the system Hamiltonian $\hat{H}$ is shown in figure B1 for a system with $L = 4$ sites at half filling and as a function of the cavity coupling g. The eigenvalues are in very good agreement for large values of $U = \Omega$, and their differences are of the order of higher-order corrections $\mathcal{O}(g^2/U,\ t^2/U,\ gt/U)$ that are neglected in equation (B1).

Appendix C. Spectrum of $\hat{H}_{D-P}$

Here we investigate the spectrum of the Hamiltonian $\hat{H}_{D-P}$ in equation (19). To this end we consider matrix elements of $\hat{H}_{D-P}$ between states in the $\hat{\mathcal{P}}_1$ manifold. Note that $\hat{H}_{D-P}$ can only couple states with one photon and no doublon to states with no photon and one doublon. In a first step, we construct electronic states $|e_j\rangle$ with exactly one doublon from the eigenstates $|g_j\rangle$ of $\hat{H}_{\rm S}$ with non-zero eigenvalue $\mathcal{E}_j < 0$,

$$|e_j\rangle = \frac{1}{2\epsilon_j}\hat{\mathcal{D}}^\dagger|g_j\rangle, \tag{C1}$$

where $\hat{\mathcal{D}}$ and ϵ_j are defined in equations (21) and (26), respectively. At half filling it is straightforward to prove the operator identity

$$\hat{\mathcal{D}}\hat{\mathcal{D}}^{\dagger} = -\frac{4}{J_c}\hat{H}_{\rm S} \tag{C2a}$$

$$= 4\hat{\mathcal{P}}_0^D\left(\sum_{\langle kl\rangle}\hat{b}_{kl}^{\dagger}\hat{b}_{kl}\right)\hat{\mathcal{P}}_0^D, \tag{C2b}$$

and hence the states $|e_j\rangle$ are orthonormal

$$\langle e_i|e_j\rangle = \frac{1}{4\epsilon_i\epsilon_j}\langle g_i|\hat{\mathcal{D}}\hat{\mathcal{D}}^{\dagger}|g_j\rangle = \delta_{ij}. \tag{C3}$$

Next we define the following states in $\hat{\mathcal{P}}_1$,

$$|\psi_P^{(j)}\rangle = |g_j\rangle \otimes |1_P\rangle, \tag{C4a}$$

$$|\psi_D^{(j)}\rangle = |e_j\rangle \otimes |0_P\rangle. \tag{C4b}$$

The matrix elements of $\hat{H}_{D-P}$ with respect to these states can be found via equation (C3) and are given by

$$\langle\psi_D^{(i)}|\hat{H}_{D-P}|\psi_P^{(j)}\rangle = 2g\epsilon_i\,\delta_{ij}. \tag{C5}$$

It follows that the matrix representation of $\hat{H}_{D-P}$ reduces to a simple 2×2 block diagonal form in the states defined in equation (C4), and diagonalizing these blocks leads to the polariton states in equation (25).

It remains to show that the matrix elements in equation (C5) and their complex conjugates are the only non-zero matrix elements of $\hat{H}_{D-P}$ in $\hat{\mathcal{P}}_1$. This can be understood as follows. First, we consider states $|\psi_D^{(k)}\rangle_{\perp}$ that complement the states $|\psi_D^{(j)}\rangle$ to an orthonormal basis in $\hat{\mathcal{P}}_1^{(0)}$. Since

$$\hat{H}_{D-P}|\psi_P^{(j)}\rangle \propto |\psi_D^{(j)}\rangle \tag{C6}$$

according to equations (19) and (C1), we find

$$_{\perp}\langle\psi_D^{(k)}|\hat{H}_{D-P}|\psi_P^{(j)}\rangle = 0 \tag{C7}$$

for all values of j and k. Second, we consider the eigenstates $|g_l^0\rangle$ of $\hat{H}_{\rm S}$ with eigenvalue zero. The states

$$|\psi_P^{(l)}\rangle_{\perp} = |g_l^0\rangle \otimes |1_P\rangle \tag{C8}$$

complement the states $|\psi_P^{(l)}\rangle$ to a basis in $\hat{\mathcal{P}}_1^{(1)}$. According to equation (C2) we have

$$\langle g_l^0|\hat{\mathcal{D}}\hat{\mathcal{D}}^{\dagger}|g_l^0\rangle = 0, \tag{C9}$$

and thus $\hat{\mathcal{D}}^{\dagger}|g_l^0\rangle = 0$. It follows that all matrix elements of $\hat{H}_{D-P}$ involving $|\psi_P^{(l)}\rangle_{\perp}$ vanish

$$\langle\psi_D^{(j)}|\hat{H}_{D-P}\,|\psi_P^{(l)}\rangle_{\perp} = 0, \tag{C10a}$$

$$_{\perp}\langle\psi_D^{(k)}|\hat{H}_{D-P}\,|\psi_P^{(l)}\rangle_{\perp} = 0, \tag{C10b}$$

which concludes our proof of the spectrum of $\hat{H}_{D-P}$.

Finally, we note that the polariton states $|\psi_{D-P}^{(j)}\rangle_{\pm}$ are not coupled by the kinetic energy term $\hat{\mathcal{P}}_1^{(0)}\hat{T}\hat{\mathcal{P}}_1^{(0)}$,

$$\langle\psi_{D-P}^{(i)}|_{\pm}\hat{\mathcal{P}}_1^{(0)}\hat{T}\hat{\mathcal{P}}_1^{(0)}\,|\psi_{D-P}^{(j)}\rangle_{\pm} \propto \langle e_i|\hat{\mathcal{P}}_1^{(0)}\hat{T}|e_j\rangle = 0. \tag{C11}$$

The second equality in equation (C11) follows from the fact that in $|e_i\rangle$, the doubly occupied site has an adjacent empty site to its right or left. On the other hand, $\hat{\mathcal{P}}_1^{(0)}\hat{T}|e_j\rangle$ is either zero or describes a state where the doublon and the holon are separated by a singly occupied site, and hence this state is orthogonal to $|e_i\rangle$.

Note that $\hat{\mathcal{P}}_1^{(0)}\hat{T}\hat{\mathcal{P}}_1^{(0)}$ has non-zero matrix elements between the states $|\psi_D^{(k)}\rangle_{\perp}$ that form the quasi-continuum of the first Hubbard band. Furthermore, $\hat{\mathcal{P}}_1^{(0)}\hat{T}\hat{\mathcal{P}}_1^{(0)}$ couples $|\psi_D^{(k)}\rangle_{\perp}$ to the polariton states $|\psi_{D-P}^{(j)}\rangle_{\pm}$ via the states $|\psi_D^{(j)}\rangle$. This coupling leads to a broadening of the polariton states but becomes less effective if the polariton splitting exceeds the tunnelling amplitude t. We thus expect the resonances in the optical conductivity to become sharper when the collective coupling increases.

Appendix D. Dicke model

The Tavis–Cummings or Dicke Hamiltonian for a system of L independent two-level atoms interacting with a single cavity mode and in rotating-wave approximation is given by [1, 2, 43, 44]

$$H_{\rm Dicke} = \Omega\hat{a}^{\dagger}\hat{a} + US_z + g(a^{\dagger}S_- + aS_+), \tag{D1}$$

where g is the light–matter coupling constant. The collective atomic operators are defined as

$$S_z = \frac{1}{2}\sum_{k=1}^{L}(|e_k\rangle\langle e_k| - |g_k\rangle\langle g_k|), \tag{D2a}$$

$$S_+ = \sum_{k=1}^{L}|e_k\rangle\langle g_k|, \tag{D2b}$$

$$S_- = S_+^\dagger = \sum_{k=1}^{L}|g_k\rangle\langle e_k|, \tag{D2c}$$

where $|g_k\rangle$ ($|e_k\rangle$) denotes the ground (excited) state for the kth atom. There are two eigenstates of $H_{\rm Dicke}$ in the subspace of one excitation, and their energy difference for $\Omega = U$ is $g_{\rm eff}$[Dicke] defined in equation (35).

ORCID iDs

Martin Kiffner https://orcid.org/0000-0002-8321-6768
Dieter Jaksch https://orcid.org/0000-0002-9704-3941

References

[1] Dicke R H 1954 Coherence in spontaneous radiation processes *Phys. Rev.* **93** 99
[2] Garraway B M 2011 The dicke model in quantum optics: Dicke model revisited *Phil. Trans. R. Soc.* A **369** 1137
[3] Fleischhauer M, Imamoğlu A and Marangos J P 2005 Electromagnetically induced transparency: optics in coherent media *Rev. Mod. Phys.* **77** 633
[4] Deng H, Haug H and Yamamoto Y 2010 Exciton-polariton Bose–Einstein condensation *Rev. Mod. Phys.* **82** 1489
[5] Carusotto I and Ciuti C 2013 Quantum fluids of light *Rev. Mod. Phys.* **85** 299
[6] Orgiu E *et al* 2015 Conductivity in organic semiconductors hybridized with the vacuum field *Nat. Mater.* **14** 1123
[7] Schwartz T, Hutchison J A, Genet C and Ebbesen T W 2011 Reversible switching of ultrastrong light-molecule coupling *Phys. Rev. Lett.* **106** 196405
[8] Kèna-Cohen S, Maier S A and Bradley D D C 2013 Ultrastrongly coupled exciton-polaritons in metal-clad organic semiconductor microcavities *Adv. Opt. Mater.* **1** 827
[9] Zhang X, Zou C-L, Jiang L and Tang H X 2014 Strongly coupled magnons and cavity microwave photons *Phys. Rev. Lett.* **113** 156401
[10] Tabuchi Y, Ishino S, Ishikawa T, Yamazaki R, Usami K and Nakamura Y 2014 Hybridizing ferromagnetic magnons and microwave photons in the quantum limit *Phys. Rev. Lett.* **113** 083603
[11] Yao B M, Gui Y S, Xiao Y, Guo H, Chen X S, Lu W, Chien C L and Hu C-M 2015 Theory and experiment on cavity magnon-polariton in the one-dimensional configuration *Phys. Rev.* B **92** 184407
[12] Sivarajah P, Lu J, Xiang M, Kamba S, Cao S and Nelson K 2016 Terahertz-frequency magnon-phonon-polaritons in the strong coupling regime arXiv:1611.01814v3
[13] Abdurakhimov L V, Khan S, Panjwani N A, Breeze J D, Seki S, Tokura Y, Morton J J L and Kurebayashi H 2018 Strong coupling between magnons in a chiral magnetic insulator Cu_2OSeO_3 and microwave cavity photons arXiv:1802.07113v1
[14] Mergenthaler M *et al* 2017 Strong coupling of microwave photons to antiferromagnetic fluctuations in an organic magnet *Phys. Rev. Lett.* **119** 147701
[15] Hagenmüller D, De Liberato S and Ciuti C 2010 Ultrastrong coupling between a cavity resonator and the cyclotron transition of a two-dimensional electron gas in the case of an integer filling factor *Phys. Rev.* B **81** 235303
[16] Scalari G *et al* 2012 Ultrastrong coupling of the cyclotron transition of a 2D electron gas to a THz metamaterial *Science* **335** 1323
[17] Zhang Q, Lou M, Li X, Reno J L, Pan W, Watson J D, Manfra M J and Kono J 2016 Collective non-perturbative coupling of 2D electrons with high-quality-factor terahertz cavity photons *Nat. Phys.* **12** 1005
[18] Li X, Bamba M, Zhang Q, Fallahi S, Gardner G C, Gao W, Lou M, Yoshioka K, Manfra M J and Kono J 2018 Vacuum Bloch–Siegert shift in Landau polaritons with ultra-high cooperativity *Nat. Photon.* **12** 324
[19] Paravicini-Bagliani G L *et al* 2019 Magneto-transport controlled by landau polariton states *Nat. Phys.* **15** 186
[20] Bartolo N and Ciuti C 2018 Vacuum-dressed cavity magnetotransport of a 2d electron gas *Phys. Rev.* B **98** 205301
[21] Editorial 2016 The rise of quantum materials *Nat. Phys.* **12** 105
[22] Powell B J and McKenzie R H 2006 Strong electronic correlations in superconducting organic charge transfer salts *J. Phys.: Condens. Matter* **18** R827
[23] Powell B J and McKenzie R H 2011 Quantum frustration in organic Mott insulators: from spin liquids to unconventional superconductors *Rep. Prog. Phys.* **74** 056501
[24] Kato R 2004 Conducting metal dithiolene complexes: structural and electronic properties *Chem. Rev.* **104** 5319
[25] Mott N F 1949 The basis of the electron theory of metals, with special reference to the transition metals *Proc. Phys. Soc.* A **62** 416
[26] Imada M, Fujimori A and Tokura Y 1998 Metal–insulator transitions *Rev. Mod. Phys.* **70** 1039
[27] Essler F H L, Frahm H, Göhmann F, Klümper A and Korepin V E 2005 *The One-Dimensional Hubbard Model* (Cambridge: Cambridge University Press)
[28] Mentink J, Balzer K and Eckstein M 2015 Ultrafast and reversible control of the exchange interaction in Mott insulators *Nat. Commun.* **6** 6708
[29] Coulthard J R, Clark S R, Al-Assam S, Cavalleri A and Jaksch D 2017 Enhancement of superexchange pairing in the periodically driven Hubbard model *Phys. Rev.* B **96** 085104
[30] Görg F, Messer M, Sandholzer K, Jotzu G, Desbuquois R and Esslinger T 2018 Enhancement and sign change of magnetic correlations in a driven quantum many-body system *Nature* **553** 481
[31] Stepanov E A, Dutreix C and Katsnelson M I 2017 Dynamical and reversible control of topological spin textures *Phys. Rev. Lett.* **118** 157201

[32] Mazza G and Georges A 2019 Superradiant quantum materials *Phys. Rev. Lett.* **122** 017401
[33] Laplace Y, Fernandez-Pena S, Gariglio S, Triscone J M and Cavalleri A 2016 Proposed cavity Josephson plasmonics with complex-oxide heterostructures *Phys. Rev.* B **93** 075152
[34] Schlawin F, Cavalleri A and Jaksch D 2019 Cavity-mediated electron–photon superconductivity *Phys. Rev. Lett.* **122** 133602
[35] Curtis J B, Raines Z M, Allocca A A, Hafezi M and Galitski V M 2019 Cavity quantum Eliashberg enhancement of superconductivity *Phys. Rev. Lett.* **122** 167002
[36] Sentef M A, Ruggenthaler M and Rubio A 2018 Cavity quantum-electrodynamical polaritonically enhanced electron–phonon coupling and its influence on superconductivity *Sci. Adv.* **4** eaau6969
[37] Kiffner M, Coulthard J R, Schlawin F, Ardavan A and Jaksch D 2019 Manipulating quantum materials with quantum light *Phys. Rev.* B **99** 085116
[38] Kiffner M, Coulthard J R, Schlawin F, Ardavan A and Jaksch D 2019 Erratum: Manipulating quantum materials with quantum light [Phys. Rev. B 99 , 085116 (2019)] *Phys. Rev.* B **99** 099907
[39] Raizen M G, Thompson R J, Brecha R J, Kimble H J and Carmichael H J 1989 Normal-mode splitting and linewidth averaging for two-state atoms in an optical cavity *Phys. Rev. Lett.* **63** 240
[40] Thompson R J, Rempe G and Kimble H J 1992 Observation of normal-mode splitting for an atom in an optical cavity *Phys. Rev. Lett.* **68** 1132
[41] Baumann K, Guerlin C, Brennecke F and Esslinger T 2010 Dicke quantum phase transition with a superfluid gas in an optical cavity *Nature* **464** 1301
[42] Migdalek J and Kim Y-K 1998 Core polarization and oscillator strength ratio anomaly in potassium, rubidium and caesium *J. Phys. B: At. Mol. Opt. Phys.* **31** 1947
[43] Tavis M and Cummings F W 1968 Exact solution for an n-molecule-radiation-field Hamiltonian *Phys. Rev.* **170** 379
[44] Tavis M and Cummings F W 1969 Approximate solutions for an n-molecule-radiation-field Hamiltonian *Phys. Rev.* **188** 692
[45] Muñoz C S, Nori F and De Liberato S 2018 Resolution of superluminal signalling in non-perturbative cavity quantum electrodynamics *Nat. Commun.* **9** 1924
[46] Cohen-Tannoudji C, Dupont-Roc J and Grynberg G 1998 *Atom-Photon Interactions* (New York: Wiley)
[47] Gallagher F B and Mazumdar S 1997 Excitons and optical absorption in one-dimensional extended Hubbard models with short- and long-range interactions *Phys. Rev.* B **56** 15025
[48] Jeckelmann E 2003 Optical excitations in a one-dimensional Mott insulator *Phys. Rev.* B **67** 075106
[49] Hochbruck M and Lubich C 1997 On Krylov subspace approximations to the matrix exponential operator *SIAM J. Numer. Anal.* **34** 1911
[50] Hasegawa T, Kagoshima S, Mochida T, Sugiura S and Iwasa Y 1997 Electronic states and anti-ferromagnetic order in mixed-stack charge-transfer compound (BEDT-TTF) (F_2 TCNQ) *Solid State Commun.* **103** 489
[51] Hasegawa T, Mochida T, Kondo R, Kagoshima S, Iwasa Y, Akutagawa T, Nakamura T and Saito G 2000 Mixed-stack organic charge-transfer complexes with intercolumnar networks *Phys. Rev.* B **62** 10059
[52] Wall S *et al* 2011 Quantum interference between charge excitation paths in a solid-state mott insulator *Nat. Phys.* **7** 114
[53] Mitrano M *et al* 2014 Pressure-dependent relaxation in the photoexcited Mott insulator ET-F_2TCNQ: influence of hopping and correlations on quasiparticle recombination rates *Phys. Rev. Lett.* **112** 117801
[54] Keller J, Scalari G, Cibella S, Maissen C, Appugliese F, Giovine E, Leoni R, Beck M and Faist J 2017 Few-electron ultrastrong light–matter coupling at 300 GHz with nanogap hybrid LC microcavities *Nano Lett.* **17** 7410
[55] Strohmaier N, Greif D, Jördens R, Tarruell L, Moritz H, Esslinger T, Sensarma R, Pekker D, Altman E and Demler E 2010 Observation of elastic doublon decay in the Fermi–Hubbard model *Phys. Rev. Lett.* **104** 080401
[56] Schuster I, Kubanek A, Fuhrmanek A, Puppe T, Pinkse P W H, Murr K and Rempe G 2008 Nonlinear spectroscopy of photons bound to one atom *Nat. Phys.* **4** 382
[57] Kishida H, Matsuzaki H, Okamoto H, Manabe T, Yamashita M, Taguchi Y and Tokura Y 2000 Gigantic optical nonlinearity in one-dimensional Mott–Hubbard insulators *Nature* **405** 929
[58] Mossel J 2008 Dynamics of the antiferromagnetic Heisenberg spin-1/2 chain *Master's Thesis* University of Amsterdam